

Internal nanoparticle structure of temperature-responsive self-assembled PNIPAM-b-PEG-b-PNIPAM triblock copolymers in aqueous solutions: NMR, SANS and light scattering studies

Article

Accepted Version

Filippov, S. K., Bogomolova, A., Kaberov, L., Velychkivska, N., Starovoytova, L., Cernochova, Z., Rogers, S. E., Lau, W. M., Khutoryanskiy, V. V. ORCID: <https://orcid.org/0000-0002-7221-2630> and Cook, M. T. (2016) Internal nanoparticle structure of temperature-responsive self-assembled PNIPAM-b-PEG-b-PNIPAM triblock copolymers in aqueous solutions: NMR, SANS and light scattering studies. *Langmuir*, 32 (21). pp. 5314-5323. ISSN 1520-5827 doi: <https://doi.org/10.1021/acs.langmuir.6b00284> Available at <https://centaur.reading.ac.uk/65646/>

It is advisable to refer to the publisher's version if you intend to cite from the work. See [Guidance on citing](#).

To link to this article DOI: <http://dx.doi.org/10.1021/acs.langmuir.6b00284>

Publisher: American Chemical Society

All outputs in CentAUR are protected by Intellectual Property Rights law, including copyright law. Copyright and IPR is retained by the creators or other copyright holders. Terms and conditions for use of this material are defined in the [End User Agreement](#).

www.reading.ac.uk/centaur

CentAUR

Central Archive at the University of Reading

Reading's research outputs online

Internal nanoparticle structure of temperature-responsive self-assembled PNIPAM-b-PEG-b-PNIPAM triblock copolymers in aqueous solutions: NMR, SANS and Light Scattering studies

Sergey K. Filippov, Anna Yurevna Bogomolova, Leonid Kabarov, Nadiia Velychkivska, Larisa Starovoytova, Zulfia Cernochova, Sarah E. Rogers, Wing Man Lau, Vitaliy V. Khutoryanskiy, and Michael T. Cook

Langmuir, **Just Accepted Manuscript** • DOI: 10.1021/acs.langmuir.6b00284 • Publication Date (Web): 09 May 2016

Downloaded from <http://pubs.acs.org> on May 16, 2016

Just Accepted

“Just Accepted” manuscripts have been peer-reviewed and accepted for publication. They are posted online prior to technical editing, formatting for publication and author proofing. The American Chemical Society provides “Just Accepted” as a free service to the research community to expedite the dissemination of scientific material as soon as possible after acceptance. “Just Accepted” manuscripts appear in full in PDF format accompanied by an HTML abstract. “Just Accepted” manuscripts have been fully peer reviewed, but should not be considered the official version of record. They are accessible to all readers and citable by the Digital Object Identifier (DOI®). “Just Accepted” is an optional service offered to authors. Therefore, the “Just Accepted” Web site may not include all articles that will be published in the journal. After a manuscript is technically edited and formatted, it will be removed from the “Just Accepted” Web site and published as an ASAP article. Note that technical editing may introduce minor changes to the manuscript text and/or graphics which could affect content, and all legal disclaimers and ethical guidelines that apply to the journal pertain. ACS cannot be held responsible for errors or consequences arising from the use of information contained in these “Just Accepted” manuscripts.

1
2
3
4
5
6
7
8
9
10
11
12
13
14
15
16
17
18
19
20
21
22
23
24
25
26
27
28
29
30
31
32
33
34
35
36
37
38
39
40
41
42
43
44
45
46
47
48
49
50
51
52
53
54
55
56
57
58
59
60

Internal nanoparticle structure of temperature-responsive self-assembled PNIPAM-*b*-PEG-*b*-PNIPAM triblock copolymers in aqueous solutions: NMR, SANS and Light Scattering studies

Sergey K. Filippov^{*,†}, *Anna Bogomolova*[†], *Leonid Kaberov*[†], *Nadiia Velychkivska*[†], *Larisa Starovoytova*[†], *Zulfiya Cernochova*[†], *Sarah E. Rogers*[‡], *Wing Man Lau*^{||}, *Vitaliy V. Khutoryanskiy*^{||}, *Michael T. Cook*^{*,⊥}

[†]Institute of Macromolecular Chemistry, AS CR, Heyrovsky Sq. 2, Prague, Prague 6, 162 06, Czech Republic.

[‡]ISIS-STFC, Rutherford Appleton Laboratory, Chilton, OX11 0QX, Oxon, United Kingdom

^{||} School of Pharmacy, University of Reading, Whiteknights, PO Box 224, Reading, Berkshire, United Kingdom, RG6 6AD

[⊥] Department of Pharmacy & Research Centre in Topical Drug Delivery and Toxicology, University of Hertfordshire, Hatfield, Hertfordshire, United Kingdom, AL10 9AB

1
2
3 KEYWORDS: nanoparticles, copolymers; NMP; SANS; self-assembly; PNIPAM; microgel;
4
5 light scattering
6
7
8
9

10
11
12 ABSTRACT
13

14
15
16 In this study we report detailed information on the internal structure of PNIPAM-*b*-PEG-*b*-
17
18 PNIPAM nanoparticles formed from self-assembly in aqueous solutions upon increase in
19
20 temperature. NMR spectroscopy, light scattering and small-angle neutron scattering (SANS)
21
22 were used to monitor different stages of nanoparticle formation as a function of temperature,
23
24 providing insight into the fundamental processes involved. The presence of PEG in a
25
26 copolymer structure significantly affects the formation of nanoparticles, making their
27
28 transition to occur over a broader temperature range. The crucial parameter that controls the
29
30 transition is the ratio of PEG/PNIPAM. For pure PNIPAM, the transition is sharp; the higher
31
32 the PEG/PNIPAM ratio results in a broader transition. This behavior is explained by different
33
34 mechanisms of PNIPAM block incorporation during nanoparticle formation at different
35
36 PEG/PNIPAM ratios. Contrast variation experiments using SANS show that the structure of
37
38 nanoparticles above cloud point temperatures for PNIPAM-*b*-PEG-*b*-PNIPAM copolymers is
39
40 drastically different from the structure of PNIPAM mesoglobules. In contrast with pure
41
42 PNIPAM mesoglobules, where solid-like particles and chain network with a mesh size of 1-3
43
44 nm are present; nanoparticles formed from PNIPAM-*b*-PEG-*b*-PNIPAM copolymers have
45
46 non-uniform structure with “frozen” areas interconnected by single chains in Gaussian
47
48 conformation. SANS data with deuterated “invisible” PEG blocks imply that PEG is
49
50 uniformly distributed inside of a nanoparticle. It is kinetically flexible PEG blocks which
51
52 affect the nanoparticle formation by prevention of PNIPAM microphase separation.
53
54
55
56
57
58
59
60

INTRODUCTION

Temperature-responsive polymers are a class of materials which undergo phase changes upon heating or cooling their solutions. If a polymer displays an expanded coil to globule transition during heating, associated with reduced solubility, it is said to display cloud point temperature (CPT). A phase diagram for aqueous solutions of temperature-responsive polymers is characterized by so-called lower critical solution temperature (LCST).^{1,2} This transition occurs due to an unfavourable entropy of mixing. A polymer reaching its CPT is usually associated with an increase in solution turbidity due to the collapse of the expanded coil, resulting in a globule which is able to phase separate via a mesoglobular state, which subsequently scatters light. For a homopolymer, the final result of reaching the CPT is polymer phase separation in solution. In block copolymer solutions, however, the phase separation of one block can result in the formation of a self-assembled structure – including micelles,³⁻¹⁰ worm-like micelles,¹¹ and gels.¹² These self-assembled structures have potential use in drug delivery, releasing their load in a temperature-dependent fashion.¹³

Poly(N-isopropyl acrylamide) (PNIPAM) is one of the most highly studied temperature-responsive polymers exhibiting a LCST. The LCST of a PNIPAM homopolymer is approximately 32°C, though copolymerization with hydrophilic monomers may alter this, as well as changes in concentration, ionic strength, and pH.¹⁴ Diblock copolymers of poly(ethylene glycol) (PEG) and PNIPAM are able to form micelles,¹⁵⁻¹⁸ vesicles,^{19,20} and gels,^{21,22} depending on molecular weights and concentration. It was established that vesicles are formed from a three-level intermediate hierarchical structure that exist in solution below CPT.²⁰ ABA triblock copolymers of PNIPAM-*b*-PEG-*b*-PNIPAM have been less studied,^{22,23} and are known to form both micelles¹⁵ and gels.^{21,22} At high concentrations of block copolymer (> 20 wt.%), gels are formed, depending on the molecular weight of each block.²¹ At lower concentrations shorter block length is detrimental to gel formation. Topp et al¹⁵ used cerium to initiate chain growth of PNIPAM (1.6 kDa) from PEG (6 kDa) to give ABA

1
2
3 triblock copolymers which assembled into micelles above 30.9°C. This was not an extensive
4
5 study, but to our knowledge is the first report of these materials. However, the effect of
6
7 molecular weight of each block was not determined. Previously, Hennik *et.al.*²³ studied
8
9 PNIPAM-*b*-PEG-*b*-PNIPAM copolymers and the presence of flower-like micelles in solution
10
11 was reported above CPT in contrast with ordinary micelles formed by PEG-*b*-PNIPAM
12
13 copolymers. Existence of loops in flower-like micelles was convincingly demonstrated by ¹H
14
15 NMR relaxometry.²³
16
17

18
19 In this study we use small-angle neutron scattering (SANS), light scattering and NMR to
20
21 study the formation of nanoparticles from PNIPAM-*b*-PEG-*b*-PNIPAM block copolymers.
22
23 The main difference of PNIPAM-*b*-PEG-*b*-PNIPAM block copolymers reported here from
24
25 ones reported in references^{19,20,23} is much shorter length of PNIPAM block. This allows for
26
27 comprehensive study of the internal structure of these self-assembled nanostructures, as well
28
29 as the other features occurring during self-assembly.
30
31

32 33 34 **Materials**

35 Tris(2-aminoethyl)amine (TREN), polyethylene glycol (PEG, 4 kDa), α -bromoisobutyryl
36
37 bromide (BIBB), formic acid, formaldehyde, N-isopropyl acrylamide (NIPAM), and copper
38
39 (I) chloride were purchased from Sigma-Aldrich (U.K.). Deuterated PEG (3.5 kDa) was
40
41 purchased from Polymer Source (Canada). Dialysis membranes with a 3.5 kDa molecular
42
43 weight cut-off (MWCO) were purchased from Visking (U.K.) and soaked for 1 h in deionized
44
45 water prior to use. Toluene and triethylamine were dried over 3 Å molecular sieves for 24 h
46
47 prior to use.
48
49

50 51 52 **Methods**

53 54 55 **Synthesis of PNIPAM-*b*-PEG-*b*-PNIPAM triblock copolymers via atom- 56 57 transfer radical-polymerization (ATRP)** 58 59 60

1
2
3 ATRP was conducted using the difunctionalized PEG macroinitiator and Me₆TREN
4 catalyst described above, with an initiator:catalyst:ligand ratio of 1:1:1. The ATRP procedure
5 was as follows: CuCl (12.4 mg, 125 μmol) was placed into a round-bottom flask, sealed with
6 a septum, then purged with N₂ for 20 min. A second flask was prepared containing NIPAM
7 (500 mg for 'low' Mw PNIPAM or 1.25 g for 'high' Mw PNIPAM) and PEG macroinitiator
8 (500 mg, 125 μmol). H₂O (2 mL) was added, followed by Me₆TREN (33.4 μL, 28.8 mg, 125
9 μmol). The solution was then allowed to stir at room temperature until complete dissolution
10 (c.a. 5 min). The solution containing NIPAM, macroinitiator, and ligand was then bubbled
11 through with N₂ for 20 min, at which point it was transferred to the flask containing CuCl via
12 syringe. The reaction was then allowed to proceed at room temperature for 24 h with stirring.
13 The resulting blue-green solution was concentrated *in vacuo*, dissolved in tetrahydrofuran
14 (THF) (5 mL), then passed through a short length of neutral alumina, resulted in a colourless
15 solution. This was concentrated *in vacuo* to yield a white solid, PNIPAM-b-PEG-b-PNIPAM.
16 Dialysis (MWCO 3.5 kDa) was necessary to remove residual monomers (as detected by ¹H
17 NMR). ¹H NMR (400 MHz, D₂O, δ): 3.86 (br, CH PNIPAM), 3.66 (br, CH₂ PEG), 1.97 (br,
18 CH₂ PNIPAM), 1.54 (br, CH₂ PNIPAM), 1.11 (br, CH₃ PNIPAM) ppm.
19
20
21
22
23
24
25
26
27
28
29
30
31
32
33
34
35
36
37
38

39 **Gel-permeation chromatography (GPC)**

40 GPC was conducted in order to determine polydispersity indexes (PDIs) and confirm that
41 PEG and PNIPAM blocks were bonded to each other. An Agilent 1260 Infinity GPC-SEC
42 system combined with 1 x Waters Styragel HR2 column was used. THF was used as mobile
43 phase at a flow rate of 1.0 mL min⁻¹. Polystyrene standards and samples were dissolved in
44 THF (2 mg/mL) with gentle heating to ensure complete dissolution of PEG. *M_n* values quoted
45 are determined by relative, narrow standard, calibration.
46
47
48
49
50
51
52
53

54 **Nuclear Magnetic Resonance (NMR)**

1
2
3 To characterize the behavior of the polymer system, the ^1H and ^1H spin-spin relaxation
4 times T_2 were measured using NMR spectroscopy. Relaxation NMR spectroscopy is a useful
5 tool for investigating polymer and solvent dynamics due to the fact that the transverse
6 magnetization component is sensitive to changes in the mobility of polymer segments as well
7 as the solvent.^{10, 24-26}

8
9
10
11
12
13
14 ^1H NMR measurements were performed with a Bruker Avance III 600 spectrometer
15 operating at 600.2 MHz. The integrated intensities were determined with the spectrometer
16 integration software at an accuracy of $\pm 1\%$. In all measurements, the temperature was
17 maintained at a constant value within ± 0.2 °C using a BVT 3000 temperature unit. The
18 samples were kept at the experimental temperature for at least 15 min before the
19 measurement. The measurement conditions were as follows: 90 pulses with a width of 10 μs ,
20 relaxation delay of 10 s, spectral width of 4844.961 Hz and 8 scans in the temperature range
21 17-57 °C. The ^1H spin-spin relaxation times T_2 for all components were measured using the
22 CPMG pulse sequence $90^\circ x-(t_d-180^\circ y-t_d)_n$ -acquisition with $t_d = 0.5$ ms. Each experiment
23 was conducted with 4 scans, a relaxation delay of 80 s and a spectral width of 9014.423 Hz.
24 The obtained T_2 relaxation curves were monoexponential and the fitting process made it
25 possible to determine a single value of the relaxation time. The relative error for T_2 values of
26 PNIPAM, HDO and PEG protons did not exceed $\pm 8\%$, $\pm 5\%$ and $\pm 6\%$, respectively.

27
28
29
30
31
32
33
34
35
36
37
38
39
40
41
42
43 To quantitatively characterize the phase separation, we have used the values of the phase-
44 separated fraction p obtained as

$$45$$
$$46$$
$$47$$
$$48$$
$$49$$
$$50$$
$$51$$
$$52$$
$$53$$
$$54$$
$$55$$
$$56$$
$$57$$
$$58$$
$$59$$
$$60$$
$$p(T) = 1 - \frac{I}{I_0} \quad (1)$$

where I is the integrated intensity of the given polymer signal in the spectrum of the partly
separated system and I_0 is the integrated intensity of this signal if no phase separation occurs.
For I_0 , we took values based on integrated intensities below the phase transition, using the

1
2
3 expected 1/T temperature dependence. The integrated intensities were measured ~20 min
4
5 after the corresponding temperature was reached (by heating).
6
7

8 **Small-angle neutron scattering (SANS)**

9 SANS experiments were performed on the time-of-flight Sans2d diffractometer at the ISIS
10
11 neutron facility, U.K. A simultaneous Q-range of 0.005 – 0.85 Å⁻¹ was achieved by utilizing
12
13 an incident wavelength range of 1.75 – 16.5 Å and employing an instrument set-up of L₁ = L₂
14
15 = 4m with the detector offset vertically 75 mm and sideways 305 mm. The beam diameter
16
17 was 8 mm. Each scattering data set was corrected for the detector efficiencies, sample
18
19 transmission and background scattering and converted to scattering cross-section data using
20
21 instrument specific software.²⁷ These data were placed on an absolute scale (cm⁻¹) using the
22
23 scattering from a standard sample (a solid blend of hydrogenous and perdeuterated
24
25 polystyrene) in accordance with established procedures.²⁸ All solutions for SANS
26
27 experiments were prepared using D₂O as solvent to reduce incoherent scattering. The
28
29 concentrations of all solutions was 0.5 wt.%. Scattering from pure D₂O was measured
30
31 separately and subtracted from solution scattering data.
32
33
34
35

36 **Light Scattering**

37
38 Static and Dynamic Light scattering (SLS and DLS) was performed to characterize the
39
40 micelles in dilute solutions. Initially, the pH dependency of the hydrodynamic radius of
41
42 particles, R_h , and the scattering intensity, I_s , were measured at a scattering angle of $\theta = 173^\circ$
43
44 with a Zetasizer Nano-ZS instrument, Model ZEN3600 (Malvern Instruments, UK). The DTS
45
46 (Nano) program was used to evaluate the data. It provides intensity-, volume-, and number-
47
48 weighted R_h distribution functions $G(R_h)$.²⁹ The intensity-weighted value of the apparent R_h
49
50 was chosen to monitor the temperature-dependent changes in the system.
51
52
53
54

55 **Static light scattering**

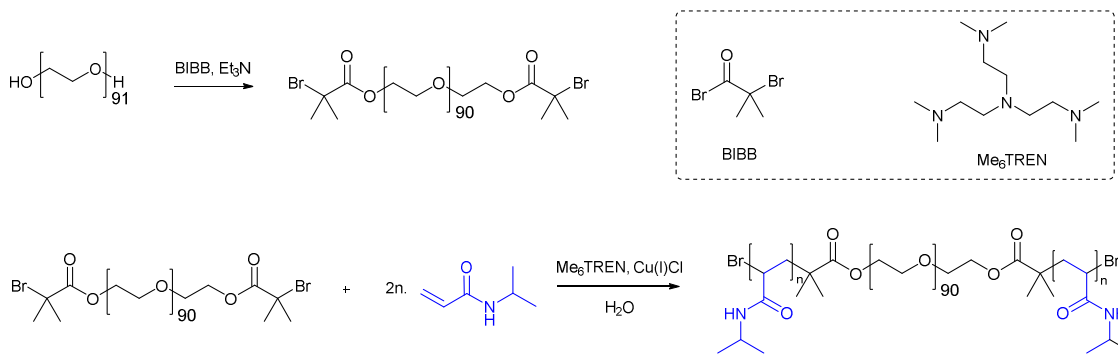
1
2
3 The static light scattering measurements were performed at 40°C in the angular range 40-
4
5 140° using ALV goniometer equipped with a 30 mW He-Ne laser ($\lambda = 632.8$ nm). Data
6
7 evaluation was carried out through using Guinier and Berry models.³⁰ The differential index
8
9 of refraction (dn/dc) was determined in a BI-DNDCW differential refractometer (Bruckhaven
10
11 Instruments Corporation) at 620.0 nm, with Differential Refractometer Software. Stock
12
13 solutions of PNIPAM-b-PEG-b-PNIPAM copolymers were prepared in D₂O (1 g/dm³). The
14
15 dn/dc value was found to be around 1.45×10^{-4} L/g.
16
17
18
19

20 21 **3D-DLS**

22
23 The aforementioned system is relatively turbid, denoting the existence of multiple scattering
24
25 contributions. Therefore the undesired multiple scattering contributions should be suppressed
26
27 in order to get reliable measurements of the form factor, in diluted solutions, or of the
28
29 structure factor in more concentrated ones.³¹⁻³³ Thus, the 3D-DLS cross-correlation technique
30
31 was used where the scattering intensity from two beams of the same wavelength
32
33 corresponding to the same scattering vector, but different scattering planes on the same
34
35 scattering volume are cross-correlated. It has been shown that contributions from multiple
36
37 scattering events is eliminated in this way, enabling us to extract information on only the
38
39 single scattering contribution. The experimental set-up which was used for both DLS and
40
41 SLS measurements is the 3D LS Spectrometer from LS instruments consisting of a
42
43 goniometer system equipped with a single laser beam (Lumentum 1145/P HeNe laser 21mW)
44
45 at 632.8nm. Experiments were conducted at 40 °C.
46
47
48
49

50 51 **RESULTS AND DISCUSSION**

52
53
54
55
56
57
58
59
60



Scheme 1. Synthetic route to PNIPAM-*b*-PEG-*b*-PNIPAM triblock copolymers

PNIPAM-*b*-PEG-*b*-PNIPAM triblock copolymers were synthesized using ATRP polymerization from a difunctionalized PEG macroinitiator (Scheme 1). This synthesis was conducted in aqueous conditions, using ME₆TREN as a ligand for a copper (I) chloride catalyst, which has been reported for the polymerization of PNIPAM.³⁴ Oxidation of copper (I) to copper (II) during the polymerization leads to the appearance of a blue-green colour solution, which was removed by passage through a short length of neutral alumina. ¹H NMR (Figure 1) showed that polymerization had occurred, with vinylic protons of the acrylamide moiety not present, replaced with alkyl protons at 1.97 and 1.54 ppm, corresponding to the polymer backbone. Additional characteristic broad peaks were identified for PNIPAM at 3.86 (CH) and 1.11 (CH₃) ppm, as well as the CH₂ protons for PEG at 3.66 ppm.

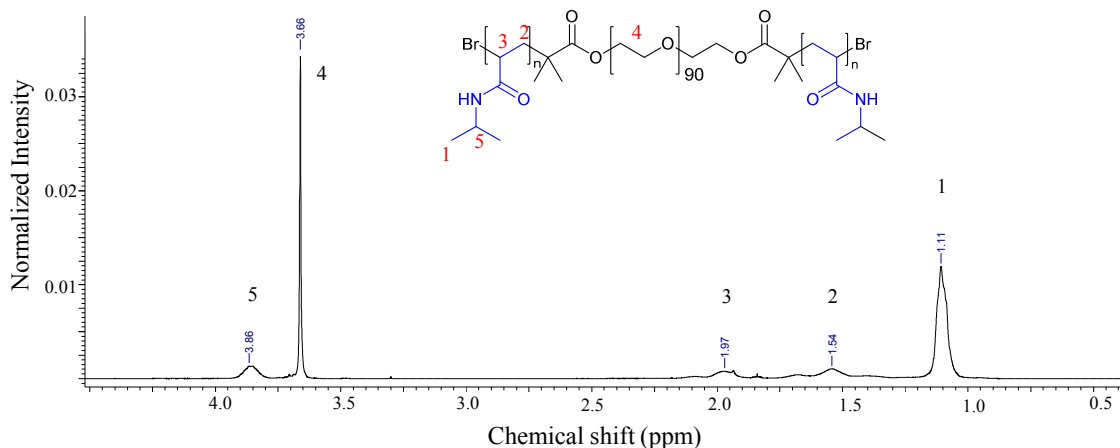


Figure 1. Exemplar ^1H NMR of PNIPAM-*b*-PEG-*b*-PNIPAM, displaying characteristic peaks of both PEG and PNIPAM.

Four samples were produced in total, in which the PEG blocks were either deuterated or non-deuterated, with PNIPAM blocks of two different molecular weights as determined by GPC (Table 1). These four samples can be grouped into two pairs. **A** and **B** have matched molecular weight deuterated-PEG and PEG blocks (3.5 and 4 kDa, respectively) and ‘short’ PNIPAM blocks (3.4 and 4.3 kDa, respectively). **C** and **D** have matched molecular weight deuterated-PEG and PEG blocks (3.5 and 4 kDa, respectively) and ‘long’ PNIPAM blocks (6.2 and 5.8 kDa, respectively). All products had satisfactory PDIs (< 1.4), considering the polydispersities of the macroinitiators.³⁴

Table 1. Molecular weight and PDI of PNIPAM-*b*-PEG-*b*-PNIPAM triblock copolymers

Sample ID	Mn (kDa)	PDI	Mn of PEG (kDa, manufacturer)	Mn of PNIPAM blocks (kDa) GPC	N of PNIPAM blocks	N of PEG blocks
A	10.3	1.4	3.5 [§]	3.4	30	79
B	12.5	1.3	4.0	4.3	38 (43*)	90
C	15.8	1.2	3.5 [§]	6.2	54	79
D	15.5	1.2	4.0	5.8	51(60*)	90

*- Data from NMR in D_2O ; [§]- PEG is deuterated

Dynamic light scattering experiments directly prove the presence of nanoparticles in solution at high temperature (Figure 2). A sharp transition is seen at the CPT of PNIPAM (approximately 35 °C), resulting in the formation of nanoparticles with a hydrodynamic radius (R_h) of approximately 75 nm. It should be noted here, that a low fraction of 200-300 nm aggregates were seen at low temperatures. This peak was discarded on Figure 2 due to concentration of these aggregates in solution is negligible. Above the CPT, the distribution was monomodal.

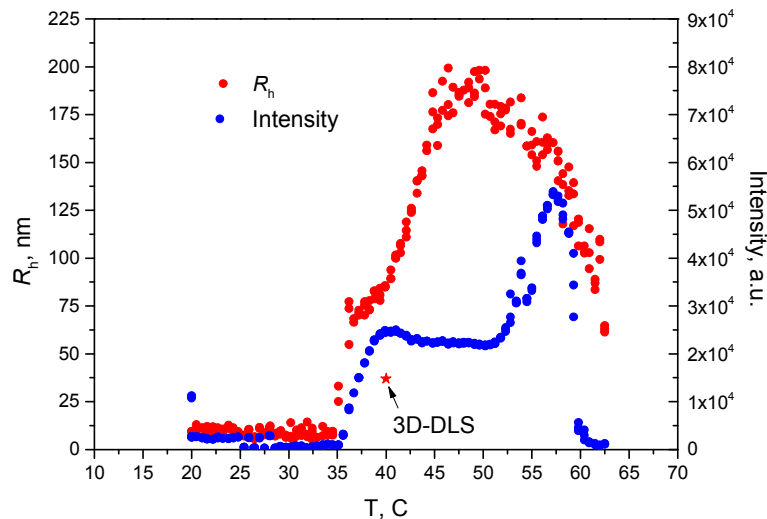


Figure 2. Temperature dependence of apparent hydrodynamic radius and scattered intensity for sample D measured using conventional DLS at $c=1.0$ wt.%. Star point indicated by arrow is the hydrodynamic radius value measured by 3D-DLS method.

Further heating above CPT, results in continuous increase in the apparent hydrodynamic radius up to 200 nm at approximately 50 °C followed by a significant drop to 50 nm. This behavior has been seen for different thermosensitive polymers such as glycogen-graft-poly(2-alkyl-2-oxazolines),³⁵ amphiphilic polyoxazolines,^{6,10} thermoresponsive nanoparticles based on poly(2-alkyl-2-oxazolines) and Pluronic F127,⁷ PNIPAM-g-PEO,³⁶ and poly(vinyl methyl

ether).³⁷ The growth of nanoparticles size can be explained by the increasing aggregation number of formed nanoparticles. At elevated temperatures, above 50°C, nanoparticle shrinks with increasing of temperature due to worsening of the thermodynamic quality of the solvent.

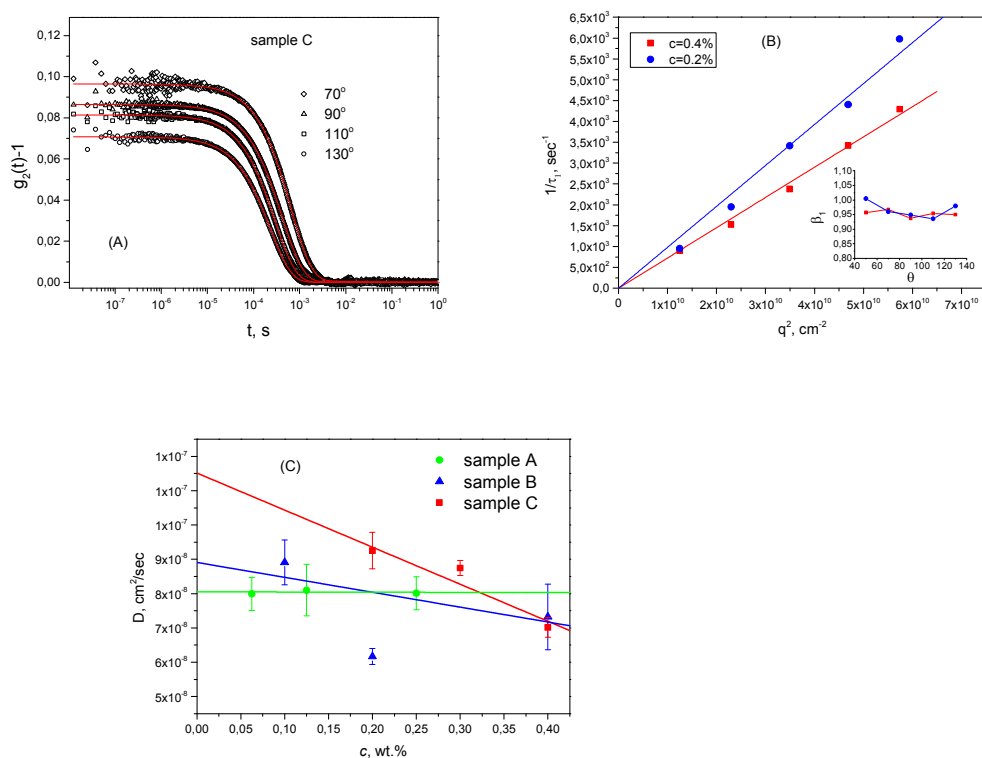


Figure 3. (A) Intensity autocorrelation functions for sample C at different angles measured by 3D-DLS method $T=40^\circ\text{C}$, $c=0.4 \text{ wt.}\%$ (B) q^2 dependence of the inverse relaxation time of the fast mode (τ_1) for sample C. Inset: angle dependence of the stretching parameter β_1 (C) Concentration dependence of apparent diffusion coefficients from 3D-DLS experiments for the fast mode (τ_1).

1
2
3 3D-DLS experiments were conducted to obtain further information on size and
4 dynamics of the nanoparticles and to investigate how apparent R_h is changing with increasing
5 concentration at 40 °C. The intensity autocorrelation functions were fitted by double
6 stretched exponential function ($A_1 \exp\left(-\left(\frac{t}{\tau_1}\right)^{\beta_1}\right) + A_2 \exp\left(-\left(\frac{t}{\tau_2}\right)^{\beta_2}\right) + B$) from where the
7 values of relaxation times were extracted (Figure 3A). Stretching parameters β_1 and β_2
8 describe polydispersity for each mode. The possible range for the β value lasts from 0 (high
9 polydispersity) to 1, for an ideal monodisperse case. Experiments were conducted in a broad
10 range of scattering angles, corresponding to scattering wave vectors q^2 from $0.5 \cdot 10^{10}$ to $5.8 \cdot$
11 10^{10} cm^{-2} . In vast majority cases, the obtained values for the amplitude for the second mode
12 (A_2) were negligible (below 0.005). That finding together with chaotic changes of
13 polydispersity parameter β_2 as a function of angle, sometimes even above 1, led us to
14 conclusion to discard the second mode from consideration. For β_1 parameter, we have
15 observed monotonous dependence in a range of 0.95-1.0 that indicates low polydispersity of
16 nanoparticles (Figure 3B, Inset). The reverse relaxation times plotted for the fast mode (τ_1) as
17 a function of q^2 indicate a diffusive nature of the relaxation process (Figure 3B) since $\frac{1}{\tau} =$
18 $D_{app} q^2$, ref ²⁶. The values of apparent diffusion coefficients were calculated from the slope
19 that were later depicted as a function of concentration (Figure 3C). From true values of
20 diffusion coefficients calculated by extrapolation to infinite dilution, the true values of
21 hydrodynamic radius were calculated for sample A, C, D. These values were different from
22 the ones measured by conventional DLS method (Figure 2). The discrepancy could be
23 attributed to the fact that conventional DLS data were measured at finite concentration. It is
24 known³⁸ that in a dilute regime the concentration dependence of a translation diffusion
25 coefficient can be written as $D_t(c) = D_0(1 + k_D c)$.
26
27 Here k_D is a second hydrodynamic virial coefficient which is specific to a particular polymer-

solvent system and depends on a product of second virial coefficient and molecular weight $k_D = 2A_2M_w - k_f - \bar{v}$. Thus the higher the molecular weights, the higher the k_D . Static light scattering support the conclusion that molecular weight of nanoparticles formed at 40 °C is very high (Table 2, Supporting information).

Table 2. Molecular weight, radius of gyration and second virial coefficient of nanoparticles at T=40 °C measured by SLS.

	A	B	C	D
	SLS	SLS	SLS	SLS
$M_w, 10^6, \text{Da}$	8.6	5.8	28	42
R_g, nm	106	107	137	124
$A_2, 10^{-9}$ mol·dm ³ /g	-4.3	2.3	0.09	-0.72

To get a deeper understanding of the internal structure of nanoparticles, NMR experiments were performed. The temperature dependence of a phase-separated fraction p , *i.e.* amount of polymer groups which take part in phase separation, was calculated for different groups (Figures 4, 5). The p value calculated for the CH₂ of PNIPAM backbone shows different behavior as a function of temperature for PNIPAM and PNIPAM-*b*-PEG-*b*-PNIPAM copolymers (Figure 4). Whereas for PNIPAM, p reaches its highest value in a very narrow temperature range, all copolymers have a much broader transition. Microphase separation for PNIPAM-*b*-PEG-*b*-PNIPAM copolymers is complex - a sharp increase is followed by gradual growth. For **C** (PNIPAM₅₄ - *b* - PEG₇₉ (D) - *b* - PNIPAM₅₄) and **D** (PNIPAM₅₁ - *b* - PEG₉₀ - *b* - PNIPAM₅₁), a first stage of transition takes place at 30 - 47 °C, with the second one at 47 - 60 °C (Figure 4A). For the backbone of block copolymers **A** (PNIPAM₃₀ - *b* - PEG₇₉ (D) - *b* - PNIPAM₃₀) and **B** (PNIPAM₃₈ - *b* - PEG₉₀ - *b* - PNIPAM₃₈), the first stage occurs at 30-57 °C, the second one at 57 - 60 °C.

A comparison of p values for the backbone and pendant groups shows that the main chain of all copolymers participates fully in phase separation, while the pendant groups of copolymers **A** and **B** collapse to the globule on 75% (Figure 4B). Nevertheless, for copolymers with longer PNIPAM chains- **C** and **D**- the p value at high temperatures shows complete phase separation for pendant groups.

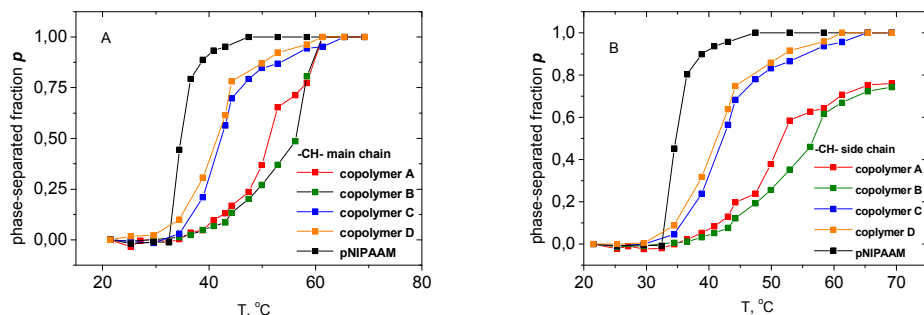


Figure 4. (A) Temperature dependence of the p -fraction as determined from integrated intensities of CH₂ band in ¹H NMR spectra of PNIPAM backbone. (B) Temperature dependence of the p -fraction as determined from integrated intensities of CH band in ¹H NMR spectra of PNIPAM pendant group.

Interestingly, PEG chains also participate in the phase-separation process (Figure 5). With increasing temperature, up to 30% of PEG groups was involved in phase separation. For the copolymers with longer PNIPAM block (**C** and **D**), the phase separation parameter for PEG groups is higher.

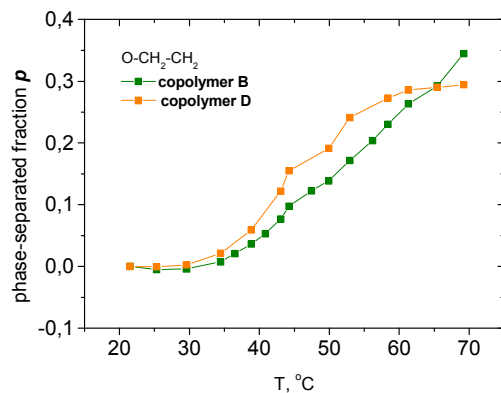


Figure 5. Temperature dependence of the p -fraction as determined from integrated intensities of PEG chains for block copolymer B and block copolymer D from ^1H NMR spectra.

Table 3. ^1H spin-spin relaxation times T_2 of CH_3 protons of a pendant group of PNIPAM, HDO molecules and CH_2 protons of PEG in D_2O solutions of PNIPAM-*b*-PEG-*b*-PNIPAM triblock copolymers.

Temperature, $^{\circ}\text{C}$	PNIPAM (s)				HDO (s)				PEG (s)			
	A	B	C	D	A	B	C	D	A	B	C	D
22	0.16	0.166	0.14	0.13	7.56	2.26	3.04	3.13	0.55	0.51	0.56	0.51
67	0.25	0.329	0.71	0.24	4.72	4.28	2.90	3.00	1.17	0.91	1.05	0.76

The local mobility data obtained from NMR experiments are in agreement with conclusions based on p value. Below the CPT, PEG chains are very mobile and T_2 relaxation time is not influenced by the presence of the different terminal PNIPAM blocks (Table 3). It is known that, ^1H spin-spin relaxation time T_2 of a specific group is proportional to its mobility, therefore PNIPAM chains are obviously much slower than PEG below CPT. The same conclusion is valid for the case above the CPT, where the similar difference between the relaxation times of PEG and PNIPAM was observed. Here it should be noted that T_2 values reported in Table 3 for PNIPAM at 67°C correspond only to a small fraction of groups that are still mobile and not involved in phase separation.

SANS

SANS experiments were conducted at 25°C (below CPT) and 40°C (above CPT). The experimental curves for all four samples are presented in Figure 6. The behavior of scattering curves at 25°C was examined first and were showing two features: a significant upturn at low $q < 0.2 \text{ nm}^{-1}$ and smooth decrease at $0.2 < q < 0.8 \text{ nm}^{-1}$. The scattered intensity for the first region for samples A and B at $q < 0.2 \text{ nm}^{-1}$ obeys a power law with $I \sim q^{-3.3}$ that corresponds

to structures with a loose surface (Figure 6A). Scattering in samples C and D have sharp interface since they manifest classical Porod behavior $I \sim q^{-4.0}$ (Figure 6B). The same approach in a q range $q > 0.2 \text{ nm}^{-1}$ reveals power law of $I \sim q^{-1.7}$. This dependency is typical for Gaussian chains with excluded volume effects. Thus, it is possible to assume that the SANS curves below CPT contain the scattering from two different structures that could be fitted by a combination of two contributions - generalized Gaussian chain form factor and mass fractal form factor: $I(q) = P_{GGC}(q) + P_{MF}(q)$. The scattering function for the generalized Gaussian coil could be written as:

$$P_{GGC}(q) = I_0^c \frac{U^{2\nu} \Gamma\left(\frac{1}{2\nu}\right) - \Gamma\left(\frac{1}{\nu}\right) - U^{2\nu} \Gamma\left(\frac{1}{2\nu}, U\right) + \Gamma\left(\frac{1}{\nu}, U\right)}{\nu U^{1/\nu}}$$

here, $U = (2\nu + 1)(2\nu + 2) \frac{q^2 R_g^2}{6}$, and $\Gamma\left(\frac{1}{2\nu}\right)$ - Gamma function.

The mass fractal form factor can be described as:

$$P_{MF}(q) = 4\pi I_0^a \int_0^\infty r^{D-3} h(r, R) \frac{\sin(qr)}{qr} r^2 dr$$

$h(r, R) = \exp\left[-\frac{Dr^2}{R_g^2}\right]$ is a cut-off function.

The choice of Gaussian chain form factor is obvious since we can expect such behavior for a single polymer chain below CPT. Concerning mass fractal contribution, there were several models which plausibly describe scattering curves at $q < 0.2 \text{ nm}^{-1}$, such as polydisperse hard spheres, fractal aggregates, *etc.*, however, mass fractal contribution gave the best fitting results. The mass fractal contribution is attributed to a small fraction of aggregates observed by DLS. Six general parameters were used in the fitting procedure; form factor: R_g^c - radius of gyration of chain, ν - excluded volume parameter or Flory exponent and I_0^c - forward scattering of chain, and mass fractal form factor with parameters: I_0^a - forward scattering of fractal aggregates, R_g^a - radius of gyration of fractal aggregates, D - fractal dimension. Results from the fit of experimental curves are shown in Table 4 and Figure 7.

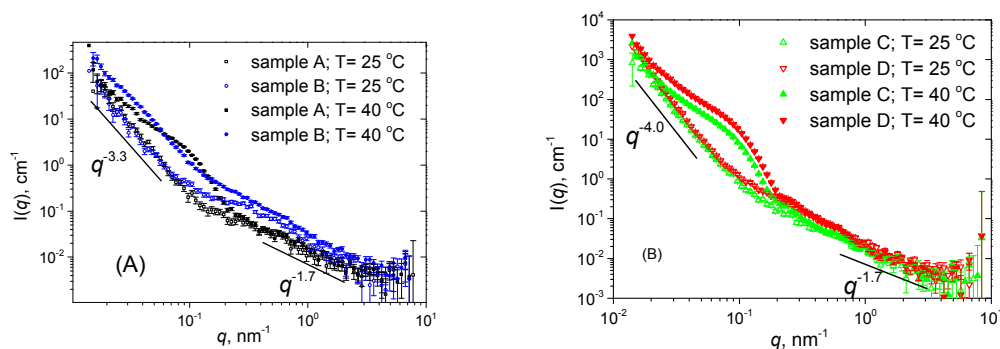


Figure 6. SANS data for PNIPAM-*b*-PEG-*b*-PNIPAM copolymers at 25 °C and 40 °C. (A) block copolymers A and B (B) block copolymers C and D.

Table 4. Fitting parameters for copolymers at 25 °C.

	A	B	C	D
Form Factor: Generalized Gaussian Coil				
R_g^c , nm	3.5±0.1	4.3±0.3	2.1±0.1	4.8±0.1
ν	0.8±0.2	0.58±0.07	0.6±0.2	0.62±0.08
I_0^s , cm ⁻¹	0.06±0.01	0.17±0.01	0.04±0.01	0.19±0.02
Structure Factor: Mass Fractal				
R_g^a , nm	66.7±0.1	97.5±0.1	105.0±0.1	105.8±0.1
D	2.58±0.02	2.51±0.02	2.75±0.01	2.78±0.01
I_0^a , cm ⁻¹	34.4±0.1	82.9±0.1	1170±1	1832±1

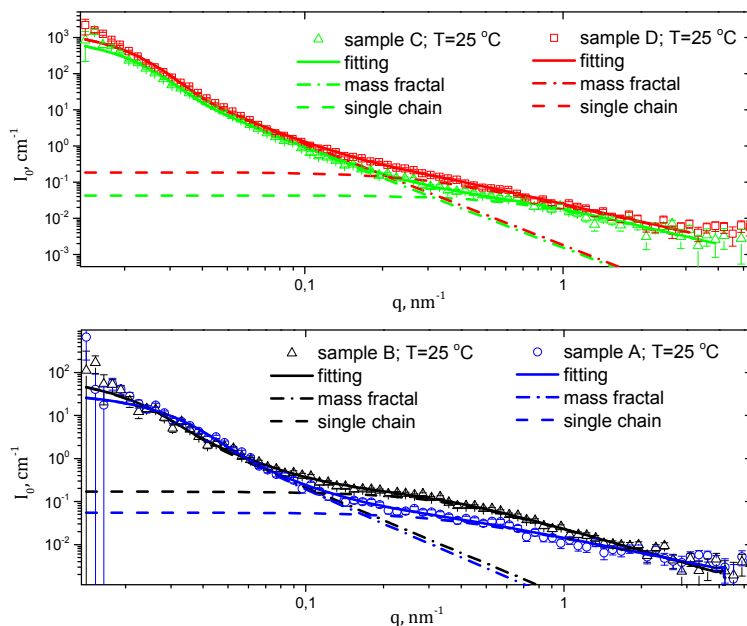


Figure 7. SANS data for polymers at 25 °C with results from the fitting procedure. Solid lines are fits.

The data obtained from the fitting procedure with those that coming from the description of chemical structure can now be compared. Several dependences could be pointed out. These features could be analyzed on different levels: on the level of single polymer chain, individual scatterers or entire particles. We shall begin our consideration with the level of polymer chain. While for the low molecular weight polymers (**A** and **B**, roughly 10-12 kDa), the variation in the length of thermoresponsive and hydrophilic block does not have significant effect on the gyration radius of single polymer chain, and the opposite was observed when molecular weight of polymer exceed 15 kDa (**C** and **D**). Thus, if we take the dimension of low molecular weight polymers as a reference, it becomes clear that the increase in the length of thermoresponsive block results in the formation of a more compact structure, even at temperature below the transition point. On the contrary, the increase in the length of

1
2
3 hydrophilic block leads to a growth in the dimensions of polymer chain. The Flory exponent
4
5 value of around 0.6 obtained from Generalized Gaussian Coil model for all polymers can be
6
7 attributed to a swollen conformation of the polymer chain; water is a thermodynamically
8
9 good solvent for our solutions at that particular temperature. Another feature appears when
10
11 we compare the radius of individual scatterers from the structure factor with the
12
13 corresponding radius of gyration of polymer chain from the form factor (Table 4). While
14
15 these values are close to each other for polymers **C** and **D**, the values from structure factor for
16
17 polymers **A** and **B** exceed the values from form factor at least in two times. One can assume,
18
19 the excluded volume has to be taken into account when the polymers **A** and **B** are analyzed.
20
21 Interestingly, the inverse correlation occurred, if we compare the content of PNIPAM groups
22
23 in polymer with dimension of individual scatters taken from the fitting results. The longer the
24
25 PNIPAM block is, the smaller size of single scatter was determined. At the same time, on the
26
27 level of whole particle, there is a well-defined relation between number of PEG units and
28
29 dimension of whole aggregate. The increase in the length of PEG block results in increase in
30
31 the size of entire aggregates. These aggregates are characterized by 2.5-2.7 fractal dimension
32
33 that corresponds to the loose cluster objects.

34
35
36
37
38 If we apply the same strategy to the analysis of scattering curves recorded at 40 °C, one
39
40 more feature should be considered in the interpretation of the experimental data; the shoulder
41
42 appears at $0.03 < q < 0.2 \text{ nm}^{-1}$. This shoulder is visible for every polymer and can be analyzed
43
44 as a result of the transition process from a molecular state of polymer at 25 °C to an aggregate
45
46 state at 40 °C. It has to be mentioned, the appearance of this shoulder in the scattering curve
47
48 diminishes partly the first region, where the significant decrease in intensity was observed
49
50 recently for curves at 25 °C, but it is still detectable at $q < 0.03 \text{ nm}^{-1}$. Thus, there are three
51
52 distinct regions here: $q < 0.03 \text{ nm}^{-1}$, $0.03 < q < 0.2 \text{ nm}^{-1}$ and $q > 0.2 \text{ nm}^{-1}$. Application of the
53
54 power law in this case gives the following results: $I_0 \sim q^{-1.4}$ for $q > 0.2 \text{ nm}^{-1}$. Definition of the
55
56
57
58
59
60

power law at values of q less than 0.03 nm^{-1} is complicated by the presence of only a few points in the region. Therefore, one can conclude that we are dealing with a very similar system. The only differences are a more compact sphere and stretched polymer chains in this particular case. For the purpose of quantitative analysis several different models have been tried for fitting. All of these models were a combination of certain form factor with MassFractal structure factor. Among form factors which were applied, i.e.: hard sphere, generalized Gaussian coil, sphere with exponential shell, sphere with attached Gaussian chains, Dozier model, the Beucage model, the only model was successful in describing the behavior of scattering curves was the Beucage mode³⁹ (Figure 8, Table 5).

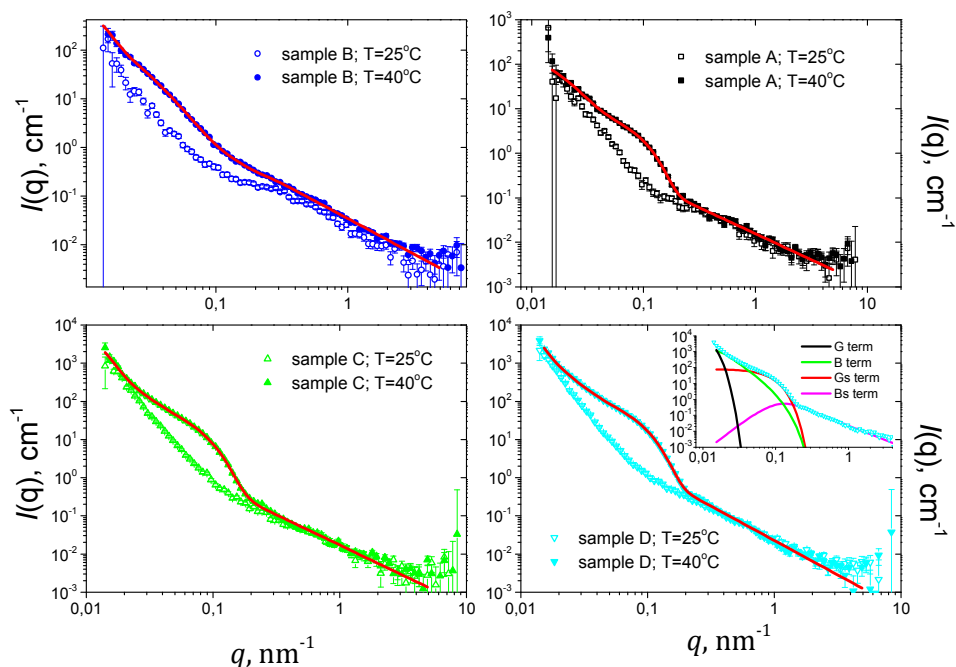


Figure 8. SANS data for every single polymer at 25 and 40 °C. Solid red lines are fits by the Beucage model. Inset for sample D: separated contributions according to the Beucage model.

Table 5. Fitting parameters for copolymers at 40 °C.

Fitting parameter of Beucage model	A d-PEG	B h-PEG	C d-PEG	D h-PEG
G	278	2061	15057	58845
B	$(1.2 \pm 1.0) \cdot 10^{-4}$	$(1.30 \pm 0.05) \cdot 10^{-2}$	$(4 \pm 1) \cdot 10^{-3}$	$(3.5 \pm 0.1) \cdot 10^{-3}$
G_s	6.2 ± 0.2	1.60 ± 0.03	40.2 ± 0.2	80.18 ± 0.01
B_s	$(1.6 \pm 0.1) \cdot 10^{-2}$	$(3.5 \pm 0.1) \cdot 10^{-2}$	$(1.7 \pm 0.1) \cdot 10^{-2}$	$(2.3 \pm 0.1) \cdot 10^{-2}$
R_{LS} , nm	156.5 ± 0.2	203.9 ± 0.1	184.6 ± 0.1	221.5 ± 0.1
R_{sub} , nm	20 ± 1	25.17 ± 0.01	14.54 ± 0.04	16.9 ± 0.1
R_s , nm	19.5	15.88 ± 0.02	24.27 ± 0.02	22.8 ± 0.1
D	3.4 ± 0.1	2.3 ± 0.1	2.9 ± 0.1	3.15 ± 0.02
D_s	1.17 ± 0.03	1.46 ± 0.01	1.58 ± 0.04	1.80 ± 0.03
χ^2	67.9	69.4	98.6	106.7

The Beucage model describes fractal aggregates consisting of smaller particles:

$$I_{BC}(q) = G \exp\left(-\frac{q^2 R_{LS}^2}{3}\right) + B \exp\left(-\frac{q^2 R_{sub}^2}{3}\right) \left(\frac{[\text{erf}(qR_s/\sqrt{6})]^3}{q}\right)^D + G_s \exp\left(-\frac{q^2 R_s^2}{3}\right) + B_s \left(\frac{[\text{erf}(qR_s/\sqrt{6})]^3}{q}\right)^{D_s}$$

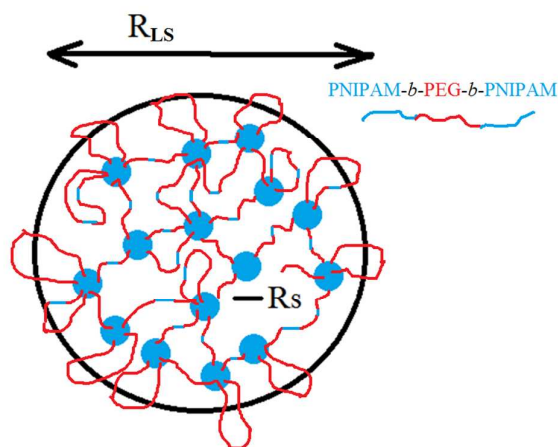
The fitting parameters for the model are G - the Guinier pre-factor of the larger structure, B - a pre-factor specific to the type of power-law scattering, G_s - the Guinier pre-factor of the smaller structure, B_s - a pre-factor specific to the type of power-law scattering, R_{LS} - large-scale structure, R_{sub} - surface-fractal cut-off radius of gyration, R_s - size of small subunits, D - scaling exponent of the power law assigned to the larger structure R_g , D_s - scaling exponent of the power law assigned to the smaller structure R_s .

There are nine fitting parameters in the Beucage model described above, and whilst all values obtained from the fitting procedure are rationalisable, we cannot completely exclude the possibility that another model could also describe the SANS data. This hypothetical model should have a similar hierarchical structure, in order to describe such a complex system.

At 40 °C, nanoparticles made of copolymer A and C have overall radius of 156 and 185 nm, respectively, consisted of small 20.3 and 14.5 nm particles, that are arranged inside of a fractal with scaling power law 3.36 and 2.89 (surface fractal). Inside of small particles, they behave as polymers with some excluded volumes effect (scaling power laws are 1.17 and 1.58) (Figure 9). Nanoparticles made of copolymers B and D are somewhat bigger than the ones composed of A and C due to protonated PEG.

NMR, DLS, and SANS data together provide an opportunity to describe nanoparticles formation in details. Below CPT, triblock copolymers exist in solution as single molecules

1
2
3 together with a small fraction of large aggregates as it nicely seen by DLS and SANS.
4 Analysis of T_2 data from NMR shows that PNIPAM blocks are less mobile in comparison
5 with a middle PEG block. Formation of nanoparticles starts from occurrence of small
6 domains formed by PNIPAM blocks since they disappear from NMR spectrum. In contrast
7
8 domains formed by PNIPAM blocks since they disappear from NMR spectrum. In contrast
9
10 with pure PNIPAM, nanoparticles formation for PNIPAM-*b*-PEG-*b*-PNIPAM expands over
11 broader temperature range and such broadening depends on the length of PEG chain. p -
12 fraction value extracted from NMR data proves that mobile PEG chains significantly retard
13 fast phase separation process. Nevertheless, at temperature much higher than CPT up to 100%
14 of all PNIPAM monomers could be inside of domains. The overall structure of nanoparticles
15 formed above CPT could be described on a large scale a surface fractal structure. PNIPAM
16 domains were visualized by SANS contrast variation study by using deuterated PEG block.
17
18
19
20
21
22
23



44
45
46
47
48
49
50
51
52
53
54
55
56
57
58
59
60

Figure 9. Hypothetical structure of nanoparticles above CPT.

CONCLUSIONS

For the first time, the onset of nanoparticles formation above CPT of PNIPAM-*b*-PEG-*b*-PNIPAM block copolymers have been analyzed in aqueous solutions in depth. The findings can be summarized as follows: below CPT, triblock copolymers exist in solution as single molecules together with a small fraction of large aggregates. PNIPAM blocks are less mobile in comparison with a middle PEG block. Formation of nanoparticles with hierarchical structure was observed above CPT. The nanoparticles could be described on a large scale a

1
2
3 surface fractal structure. On a short scale nanoparticles consist of small domains of partially
4
5 phase-separated PNIPAM blocks interconnected by mobile PEG chains. Such domains were
6
7 visualized by SANS contrast variation study by using deuterated PEG block. Further increase
8
9 in temperature above CPT leads to higher immobilization of PNIPAM blocks inside of
10
11 domains up to 100% of all monomer units.
12
13
14
15
16
17
18

19 ASSOCIATED CONTENT

22 **Supporting Information**

23
24
25
26 Synthesis of PEG macroinitiator. Synthesis of ME₆TREN. Guinier plot for the sample C. A
27
28 Guinier plot for the sample B; Temperature 40°C. Guinier plot for the sample D; Temperature
29
30 40°C
31

32 This material is available free of charge via the Internet at <http://pubs.acs.org>.”
33
34

35 AUTHOR INFORMATION

36
37
38 Corresponding Author (**Sergey Filippov**)
39

40
41 *Tel: +420-608720561; Fax: +420-296809410
42

43
44 E-mail: sfill225@gmail.com
45

46
47 Corresponding Author (**Michael T. Cook**)
48

49 *Tel: +44 (0)170 728 3439
50

51
52 E-mail: m.cook5@herts.ac.uk
53
54
55

56
57 Author Contributions
58
59
60

1
2
3 The manuscript was written through contributions of all authors. All authors have given
4 approval to the final version of the manuscript.
5
6
7

8 Notes
9

10 The authors declare no competing financial interest.
11
12

13 ACKNOWLEDGMENTS 14

15
16 The ISIS (Didcot, UK) is thanked for granting SANS beam time (experiment number
17 1410107). S.F. acknowledges the Czech Science Foundation Grant No. 15-10527J. The
18 authors acknowledge support from the European Union under the Framework 7 program
19 under a contract from an Integrated Infrastructure Initiative (Reference 262348, ESMI). S.F.
20 thanks Ms. Panagiota Bogri and Dr. George Petekidis for their help with 3D-DLS
21 experiments. The authors acknowledge Chemical Analysis Facility (University of Reading)
22 for providing access to NMR spectroscopy used in the analysis of chemical structure of
23 triblock copolymers.
24
25
26
27
28
29
30
31
32
33
34
35
36
37
38
39

40 REFERENCES 41

- 42
43 (1) Aseyev, V.; Tenhu, H.; Winnik, F. M. Non-ionic Thermoresponsive Polymers in Water.
44 *Adv. Polym. Science* **2011**, *242*, 29-89.
45
46
47
48 (2) Wang, X.; Wu, C. Light-Scattering Study of Coil-to-Globule Transition of a Poly(N-
49 isopropylacrylamide) Chain in Deuterated Water. *Macromolecules* **1999**, *32*, 4299-4301.
50
51
52
53
54
55
56
57
58
59
60

1
2
3 (3) Prabakaran, M.; Grailer, J. J.; Steeber, D. A.; Gong, S. Q. Thermosensitive micelles based
4 on folate-conjugated poly(N-vinylcaprolactam)-block-poly(ethylene glycol) for tumor-
5 targeted drug delivery. *Macromol. Biosci.* **2009**, *9*, 744–753.
6
7

8
9
10 (4) Hruby, M.; Konak, C.; Kucka, J.; Vetrik, M.; Filippov, S.K.; Vetvicka, D.; Mackova, H.;
11 Karlsson, G.; Edwards, K.; Rihova, B.; Ulbrich, K. Thermoresponsive, Hydrolytically
12 Degradable Polymer Micelles Intended for Radionuclide Delivery. *Macromol. Biosci.* **2009**,
13 *9*, 1016-1027.
14
15
16
17

18
19
20 (5) Hruby, M.; Filippov, S.K.; Panek, J.; Novakova, M.; Mackova, H.; Kucka, J.; Ulbrich, K.
21 Thermoresponsive micelles for radionuclide delivery. *J Control. Release.* **2010**, *148*, E60-
22 E62.
23
24
25
26

27 (6) Hruby, M.; Filippov, S.K.; Panek, J.; Novakova, M.; Mackova, H.; Kucka, J.; Vetvicka,
28 D.; Ulbrich, K. Polyoxazoline Thermoresponsive Micelles as Radionuclide Delivery Systems.
29 *Macromol. Biosci.* **2010**, *10*, 916-924.
30
31
32
33

34 (7) Panek, J.; Filippov, S.K.; Hruby, M.; Rabyk, M.; Bogomolova, A.; Kucka, J.; Stepanek, P.
35 Thermoresponsive Nanoparticles Based on Poly(2-alkyl-2-Oxazolines) and Pluronic F127.
36 *Macromol. Rap. Com.* **2012**, *33*, 1683-1689.
37
38
39
40
41

42 (8) Bogomolova, A.; Hruby, M.; Panek, J.; Rabyk, M.; Turner, S.; Bals, S.; Steinhart, M.;
43 Zhigunov, A.; Sedlacek, O.; Stepanek, P.; Filippov, S.K. Small-angle X-ray scattering and
44 light scattering study of hybrid nanoparticles composed of thermoresponsive triblock
45 copolymer F127 and thermoresponsive statistical polyoxazolines with hydrophobic moieties.
46
47
48
49
50
51 *J. Appl. Crystal.* **2013**, *46*, 1690-1698.
52
53
54
55
56
57
58
59
60

1
2
3 (9) Laga, R.; Janouškova, O.; Ulbrich, K.; Pola, R.; Blazkova, J.; Filippov, S.K.; Etrych T.;
4
5 Pechar, M. Thermo-responsive polymer micelles as nano-sized pharmaceuticals for cancer
6
7 therapy, *Biomacromolecules* **2015**, *16*, 2493–2505.
8

9
10 (10) Bogomolova, A.; Filippov, S.K.; Starovoytova, L.; Angelov, B.; Konarev, P.; Svergun,
11
12 D. I.; Sedlacek, O.; Hruby, M.; Stepanek, P. Study of Study of Thermosensitive
13
14 Amphiphilic Poly-Oxazolines of Complex Nature and Their Interaction with Ionic
15
16 Surfactants. Hydrophobic, Thermosensitive and Hydrophilic Moieties: Are They Equally
17
18 Important? *J Phys. Chem. B* **2014**, *118*, 4940-4950.
19

20
21 (11) Duval, M.; Waton, G.; Schosseler, F. Temperature-induced growth of wormlike
22
23 copolymer micelles. *Langmuir* **2005**, *21*, 4904–4911.
24
25

26
27 (12) Escobar-Chávez, J. J.; López-Cervantes, M.; Naik, A.; Kalia, Y.N.; Quintanar-
28
29 Guerrero, D.; Ganem-Quintanar, A. Applications of thermo-reversible pluronic F-127 gels in
30
31 pharmaceutical formulations. *J. Pharm. Pharm. Sci.* **2006**, *9*, 339–358.
32
33

34
35 (13) He, C.; Kim, S. W.; Lee, D. S. In situ gelling stimuli-sensitive block copolymer
36
37 hydrogels for drug delivery. *J. Control. Release.* **2008**, *127*, 189–207.
38
39

40
41 (14) Hoogenboom, R.; Thijs, H.M.L.; Jochems, M.J.H.C.; van Lankvelt, B.M.; Fijten,
42
43 M.W.M.; Schubert, U.S. Tuning the LCST of poly(2-oxazoline)s by varying composition and
44
45 molecular weight: alternatives to poly(N-isopropylacrylamide)? *Chem. Commun. (Camb).*
46
47 **2008**, 5758–5760.
48

49
50 (15) Topp, M. D. C.; Dijkstra, P. J.; Talsma, H.; Feijen, J. Thermosensitive Micelle-Forming
51
52 Block Copolymers of Poly(ethylene glycol) and Poly(N-isopropylacrylamide).
53
54 *Macromolecules* **1997**, *30*, 8518–8520.
55
56
57
58
59
60

1
2
3 (16) Virtanen, J.; Holappa, S.; Lemmetyinen, H.; Tenhu, H. Aggregation in Aqueous Poly(N-
4 isopropylacrylamide)-block-poly(ethylene oxide) Solutions Studied by Fluorescence
5 Spectroscopy and Light Scattering. *Macromolecules* **2002**, *35*, 4763–4769.
6
7

8
9
10 (17) Zhu, P. Particle formation and aggregation - collapse behavior of poly (N -
11 isopropylacrylamide) and poly (ethylene glycol) block copolymers in the presence of cross-
12 linking agent. *J Mater Sci Mater Med.* **2004**, *5*, 567–573.
13
14

15
16
17 (18) Zhang, W.; Shi, L.; Wu, K.; An, Y. Thermoresponsive Micellization of Poly (ethylene
18 glycol)-b -poly (N-isopropylacrylamide) in Water. *Macromolecules* **2005**, 5743–5747.
19
20

21
22 (19) Zhao, J.; Zhang, G.; Pispas S. Morphological transitions in aggregates of thermosensitive
23 poly(ethylene oxide)-b-poly(N-isopropylacrylamide) block copolymers prepared via RAFT
24 polymerization. *J. Polym. Sci. Part A: Polym. Chem.* **2009**, *47*, 4099e110.
25
26

27
28 (20) Papagiannopoulos, A.; Zhao, J.; Zhang, G.; Pispas, S.; Radulescu, A. Thermoresponsive
29 transition of a PEO-b-PNIPAM copolymer: From hierarchical aggregates to well defined
30 ellipsoidal vesicles. *Polymer*, **2013**, *54*, 6373-6380.
31
32

33
34 (21) Lin, H. H.; Cheng, Y. L. In-situ thermoreversible gelation of block and star copolymers
35 of poly(ethylene glycol) and poly(n-isopropylacrylamide) of varying architectures.
36
37 *Macromolecules* **2001**, *34*, 3710–3715.
38
39

40
41 (22) Teodorescu, M.; Negru, I.; Stanescu, P.O.; Drghici, C., Lungu, A., Sarbu, A.c
42 Thermogelation properties of poly(N-isopropylacrylamide) – block – poly(ethylene glycol) –
43 block – poly(N-isopropylacrylamide) triblock copolymer aqueous solutions. *React. Funct.*
44
45 *Polym.* **2010**, *70*, 790–797.
46
47

48
49 (23) De Graaf, A.J.; Boere, K.W.; Kemmink, J.; Fokkink, R.G.; van Nostrum, C.F.; Rijkers,
50 D.T.; van der Gucht, J.; Wienk, H.; Baldus, M.; Mastrobattista, E.; Vermonden, T.; Hennink,
51
52
53
54
55
56
57
58
59
60

1
2
3 W.E. Looped structure of flowerlike micelles revealed by ^1H NMR relaxometry and light
4 scattering. *Langmuir* **2011**, *27*, 9843-9848.

5
6
7
8 (24) Radecki, M.; Spěvák, J.; Zhigunov, A.; Sedláková, Z.; Hanyková, L. Temperature-
9 induced phase transition in hydrogels of interpenetrating networks of poly(N-
10 isopropylacrylamide) and polyacrylamide. *Eur. Polym. J.* **2015**, *68*, 68-79.

11
12
13 (25) Uřilová, H.; Čtástná, J.; Nyková, L.; Dláková, Z.; Spěvák, J. ^1H NMR study of
14 temperature-induced phase separation in solutions of poly(N-isopropylmethacrylamide-co-
15 acrylamide) copolymers. *Eur. Polym. J.* **2010**, *46*, 1299-1306.

16
17
18 (26) Spěvák, J. NMR investigations of phase transition in aqueous polymer solutions and
19 gels. *Cur. Opin. Colloid. Interf. Sci.* **2009**, *14*, 184-191.

20
21
22 (27) http://www.mantidproject.org/Main_Page

23
24
25 (28) Wignall, G. D.; Bates, F. S. Absolute calibration of small-angle neutron scattering data.
26
27
28
29
30
31
32
33
34
35
36
37
38
39
40
41
42
43
44
45
46
47
48
49
50
51
52
53
54
55
56
57
58
59
60
J. Appl. Crystallogr. **1987**, *20*, 28-40.

(29) Pecora, R. *Dynamic Light Scattering: Applications of Photon Correlation Spectroscopy*,
Plenum Press, **1985**.

(30) B. Chu, *Laser Light Scattering: Basic Principles and Practice*, Academic Press, Inc. New
York, **1991**.

(31) Urban, C.; Schurtenberger, P. Characterization of turbid colloidal suspensions using light
scattering techniques combined with cross-correlation methods, *J. Colloid Interf. Sci.* **1998**,
207, 150-158.

(32) Scheffold, F.; Schurtenberger, P. Light scattering probes of viscoelastic fluids and solids,
Soft Mater. **2003**, *1*, 139-165.

1
2
3 (33) Pusey, P.N., Suppression of multiple scattering by photon cross-correlation techniques,
4
5 *Cur. Opin. Colloid Interf. Sci.* **1999**, *4*, 177-185.
6
7

8 (34) Ye, J.; Narain, R. Water-assisted atom transfer radical polymerization of N-
9 isopropylacrylamide: nature of solvent and temperature. *J. Phys. Chem. B.* **2009**, *113*, 676-
10 681.
11
12
13

14 (35) Pospisilova, A.; Filippov, S. F.; Bogomolova, A.; Turner, S.; Sedlacek, O.; Matushkin,
15 N.; Cernochova, Z.; Stepanek P.; Hruby, M. Glycogen-graft-poly(2-alkyl-2-oxazolines) –
16 the new versatile biopolymer-based thermoresponsive macromolecular toolbox. *RSC Adv.*
17 **2014**, *4*, 61580-61588.
18
19
20
21
22
23

24 (36) Virtanen, J.; Baron, C.; Tenhu, H. Grafting of poly(N-isopropylacrylamide) with
25 poly(ethylene oxide) under various reaction conditions. *Macromolecules* **2000**, *33*, 336-341.
26
27
28

29 (37) Aseyev, V.; Hietala, S.; Laukkanen, A.; Nuopponen, M.; Confortini, O.; Du Prez, F.E.;
30 Tenhu, H. Mesoglobules of thermoresponsive polymers in dilute aqueous solutions above the
31 LCST. *Polymer* **2005**, *46*, 7118-7131.
32
33
34
35
36
37

38 (38) Yamakawa, H. Modern Theory of Polymer Solutions (Harper and Row, New York,
39 **1971**).
40
41
42

43 (39) Beaucage, G. Approximations leading to a unified exponential/power-law approach to
44 small-angle scattering. *J. Appl. Cryst.* **1995**, *28*, 717-728.
45
46
47
48
49
50
51
52
53
54
55
56
57
58
59
60

For Table of Contents Use Only

Title: Internal nanoparticle structure of temperature responsive self-assembled PNIPAM-*b*-PEG-*b*-PNIPAM triblock copolymers in aqueous solutions: NMR, SANS and Light Scattering studies

Authors: Sergey K. Filippov, Anna Bogomolova, Leonid Kaberov, Nadiia Velychkivska, Larisa Starovoytova, Zulfiya Cernochova, Sarah E. Rogers, Wing Man Lau, Vitaliy V. Khutoryanskiy, Michael T. Cook

